A Global Simulation of ICRF Heating in a 3D Magnetic Configuration

S. Murakami 1), A. Fukuyama 1), T. Akutsu 1), N. Nakajima 2), V. Chan 3), M. Choi 3), S.C. Chiu 4), L. Lao 3), V. Kasilov 5), T. Mutoh 1), R. Kumazawa 1), T. Seki 1), K. Saito 1), T. Watari 1), M. Isobe 1), T. Saida 6), M. Osakabe 1), M. Sasao 6)
and LHD Experimental Group

1) Department of Nuclear Engineering, Kyoto University, Kyoto 606-8501, Japan
2) National Institute for Fusion Science, Oroshi, Toki, Gifu 509-5292, Japan
3) General Atomics, P.O. Box 85608, San Diego, California 92186-5608, USA
4) Sunrise R&M, Inc., 8585 Hopseed Lane, San Diego, California 92129, USA
5) Institute of Plasma Physics, National Science Center, KIPT, Kharkov, Ukraine
6) Graduate School of Engineering, Tohoku University, Sendai 980-8579, Japan

e-mail contact of main author: murakami@nucleng.kyoto-u.ac.jp

Abstract. A global simulation code for the ICRF heating analysis in a three-dimensional (3D) magnetic configuration is developed combining two global simulation codes; a drift kinetic equation solver, GNET, and a wave field solver, TASK/WM. Both codes take into account 3D geometry using the numerically obtained 3D MHD equilibrium. The developed simulation code is applied to the LHD configuration as an example. Characteristics of energetic ion distributions in the phase space are clarified in LHD. The simulation results are also compared with experimental results by evaluating the count number of the neutral particle analyzer using the obtained energetic ion distribution, and a relatively good agreement is obtained.

1. Introduction

ICRF heating experiments has been successfully done in helical systems[1-7] and have demonstrated the effectiveness of this heating method in three-dimensional (3D) magnetic configurations. In LHD, a significant performance of this method have also shown[8-11] and up to 500keV of energetic tail ions have been observed by fast neutral particle analysis (NPA)[12,13]. These measured results indicate a good property of energetic ion confinement in helical systems. However, the measured information by NPA is obtained as an integrated value along a line of sight and we need a reliable theoretical model for reproducing the energetic ion distribution to discuss the confinement of energetic ions accurately.

On the other hand, ICRF heating generates highly energetic trapped ions, which drift around the torus for a long time (typically on a collisional time scale) interacting with the RF wave field. Thus, the behavior of these energetic ions is strongly affected by the characteristics of the drift motions, that depend on the magnetic field configuration. In particular, in a 3D magnetic configuration, complicated drift motions of trapped particles would play an important role in the confinement of the energetic ions and the ICRF heating process.

Many efforts have been made to analyze the energetic particle distribution and the transport during ICRF heating, analytically and numerically (Fokker-Planck model and etc.), but most of the analyses using local approximation. A simple Orbit following Monte Carlo simulation has been used to take into account the non-local effect due to finite orbit size of energetic ions[1-3]. However, the energetic particle distribution changes in time and we can not obtain a correct steady state by this type of Monte Carlo simulation[14]. To obtain a steady state we should consider the balanced state between particle source and sink correctly in a global simulation.

Additionally, since the wavelength of the ICRF heating is typically comparable to the plasma scale length and the 3D geometry effect on the RF wave field would be also important in a 3D magnetic configuration. Therefore a global simulation of ICRF heating is necessary for the accurate modeling of the plasma heating process in a 3D magnetic configuration.

In this paper we study the ICRF heating in a 3D magnetic configuration combining two global simulation codes; a drift kinetic equation solver GNET [15,16] and a wave field solver TASK/WM [17]. We apply the simulation code to the LHD configuration as an example. We make clear the characteristics of energetic ions distribution in the phase space, and also show the confinement property of LHD configurations by comparing the simulation and experimentally observed results.

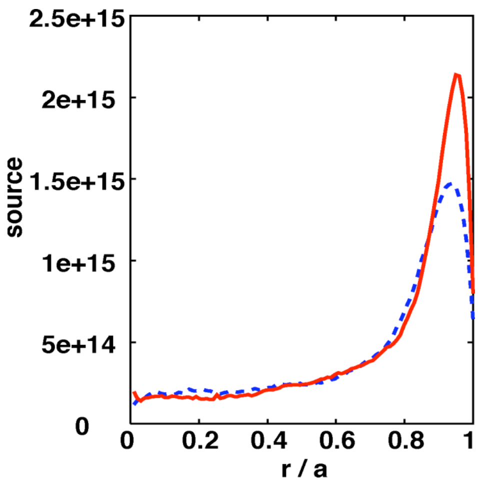

FIG. 1: Radial profiles of the minority ion sources; n_{e0}*=2.0x10*^{19}*m*$^{-3}$ *(solid line) and 1.0 x 10*^{19} *m*$^{-3}$ *(dotted line).*

2. Simulation Model

In order to study the ICRF heating in a 3D magnetic field configuration we have developed a global simulation code combining two global codes; GNET and TASK/WM.

GNET solves a linearized drift kinetic equation for energetic ions including complicated behavior of trapped particles in 5-D phase space as

where $C(f)$ and Q_{ICRF} are the linear Coulomb Collision operator and the ICRF heating term.

$$\frac{\partial f}{\partial t} + (\mathbf{v}_{//} + \mathbf{v}_D)\cdot\nabla f + \mathbf{a}\cdot\nabla_{\mathbf{v}} f - C(f) - Q_{ICRF}(f) - L_{particle} = S_{particle},$$

$S_{particle}$ is the particle source term by ionization of neutral particle and the radial profile of the source is evaluated using AURORA code. Figure 1 shows the typical profile of minority ion source for two densities. The particle sink (loss) term, $L_{particle}$, consists of two parts; one is the loss by the charge exchange loss assuming the same neutral particle profile as the source term calculation and the other is the loss by the orbit loss escaping outside of outermost flux surface.

In GNET code the minority ion distribution f is evaluated through a convolution of $S_{particle}$ with a characteristic time dependent Green function evaluated using test particle Monte Carlo method. We follows the test particle orbits to evaluate the Green function in the Boozer coordinates.

The Q_{ICRF} term is modeled by the Monte Carlo method. When the test particle pass through the resonance layer where $\omega - k_{//}v_{//} = n\omega_c$ the perpendicular velocity of this particle is changed by the following amount,

$$\Delta v_\perp = \sqrt{\left(v_{\perp 0} + \frac{q}{2m} I |E_+| J_{n-1}(k_\perp \rho)\cos\phi_r\right)^2 + \frac{q^2}{4m^2}\left\{I|E_+|J_{n-1}(k_\perp\rho)\right\}^2 \sin^2\phi_r} - v_{\perp 0}$$

$$\approx \frac{q}{2m} I |E_+| J_{n-1}(k_\perp \rho)\cos\phi_r + \frac{q^2}{8m^2 v_{\perp 0}}\left\{I|E_+|J_{n-1}(k_\perp\rho)\right\}^2 \sin^2\phi_r$$

$$I = \sqrt{2\pi/n\dot{\omega}} \;\text{ or }\; 2\pi(n\ddot{\omega}/2)^{-1/3}Ai(0)$$

This expression includes the quadratic terms in wave amplitude and the averages of $\Delta v_\perp$ and $\Delta v_\perp^2$ over the random phase we obtain up to the leading order terms,

$$\langle \Delta v_\perp \rangle \approx \frac{q^2}{16m^2 v_{0\perp}} I^2 |E_+|^2, \quad \langle \Delta v_\perp^2 \rangle \approx \frac{q^2}{8m^2} I^2 |E_+|^2$$

and the following relation is fulfilled.

$$\langle \Delta v_\perp \rangle = \frac{1}{v_{0\perp}} \frac{\partial}{\partial v_{0\perp}}\left(v_{0\perp}\frac{\langle \Delta v_\perp^2 \rangle}{2}\right)$$

The spatial profile of RF wave electric field is necessary for the accurate calculation of the ICRF heating. The profile of RF wave field is an important factor on the ICRF heating and this profiles affect the particle orbit. We evaluate the RF wave field by the TASK/WM code. TASK/WM solves Maxwell's equation for RF wave electric field, $\mathbf{E}_{RF}$, with complex frequency, ω, as a boundary value problem in the 3D magnetic configuration.

$$\nabla \times \nabla \times \mathbf{E}_{RF} = \frac{\omega^2}{c^2}\vec{\varepsilon}\cdot\mathbf{E}_{RF} + i\omega\mu_0 \mathbf{j}_{ext},$$

Here, the external current, $\mathbf{j}_{\mathrm{ext}}$, denotes the antenna current in ICRF heating. The response of the plasma is described by a dielectric tensor including kinetic effects in a local normalized orthogonal coordinates.

In the simulation, first, we solve the RF wave field assuming the minority ion distribution and then we solve the minority ion distribution by GNET. Both codes assume a 3D magnetic configuration based on the MHD equilibrium by the VMEC code.

The developed code is benchmarked with ORBIT-RF [18] for 2-D geometry applying to the DIII-D configuration.

3. Simulation Results

We apply the global simulation code to a LHD configuration (R_{ax} = 3.6m; the in-ward shifted configuration). This LHD configuration conforms the σ-optimized configuration and shows relatively good trapped particle orbit[19]. Most of ICRF heating experiments has been performed in this configuration.

The RF resonance position relative to magnetic flux surface has been tested mainly for two cases in the LHD experiments. One is the off-axis heating case in which the resonance surface almost crossing a saddle point of magnetic field at the longitudinally elongated cross section. In the off-axis case the resonance region only exists for $r/a>0.5$. The other is the on-axis heating in which the resonance surface crossing a magnetic axis. The relation between the resonance surface and flux surfaces are shown in Fig. 2. The experimentally obtained results have shown the difference in the heating efficiencies and the decrease of energetic particle neutral count number detected by natural diamond detector (NDD-NPA) [20].

We, first, apply the TASK/WM code to evaluate the RF wave electric fields (E_+ and E_-) and, then, the obtained spatial profile of the RF field is used as a RF heating term in the GNET code. The similar heating and plasma parameters as the experimental ones are assumed in the calculation.

Figure 3 shows the steady state distribution of the minority ions during ICRF heating obtained by GNET. We plot the flux surface averaged tail ion distribution in the three dimensional space (r/a, $v_{//}$, v_{perp}), where a/r, $v_{//}$ and v_{perp} are the normalized averaged minor radius, the parallel and perpendicular velocities normalized by the thermal velocity at the plasma center, respectively.

The RF wave accelerates minority ions perpendicularly in the velocity space and we can see perpendicularly elongated minority ion distributions. We find a peaked energetic tail ion distribution near r/a~0.5 in the off-axis heating case (Fig.3, left). Also, the energetic ions distribution has a triangular shape. This is because the large absorption of RF wave occurs when the banana tips of trapped particles are close to the resonance surface and those pitch angle of the particle depends on the minor radius (monotonically increase as a function of minor radius).

On the other hand we can see no strong peak in the distribution function in the on-axis heating case (Fig.3, right). The energetic particle distribution is broader than that of the off-axis case and the less energetic tail ion is obtained.

Figure 4 shows the minority ion pressure, which shows a population of energetic ions in the real space. We can see the clear difference between two heating cases. The high pressure regions are localized along the helical ripple where the magnetic field is weak and trapped particle are confined in this region. On the other hand the high pressure region is not localized and the a little stronger in the outer side (left side of the figure) of the torus.

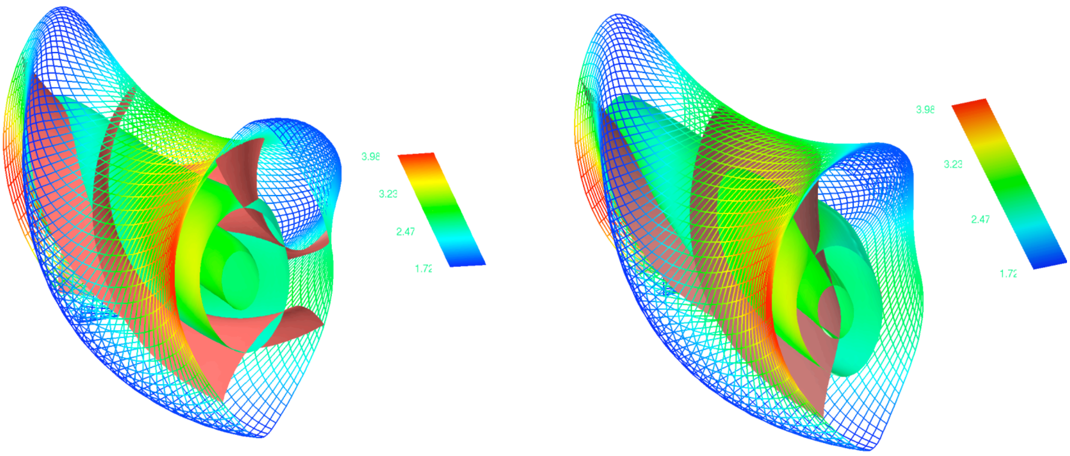

FIG. 2: 3D plots of the ICRF resonance surfaces in the off-axis point heating case (left) and on-axis heating case (right).

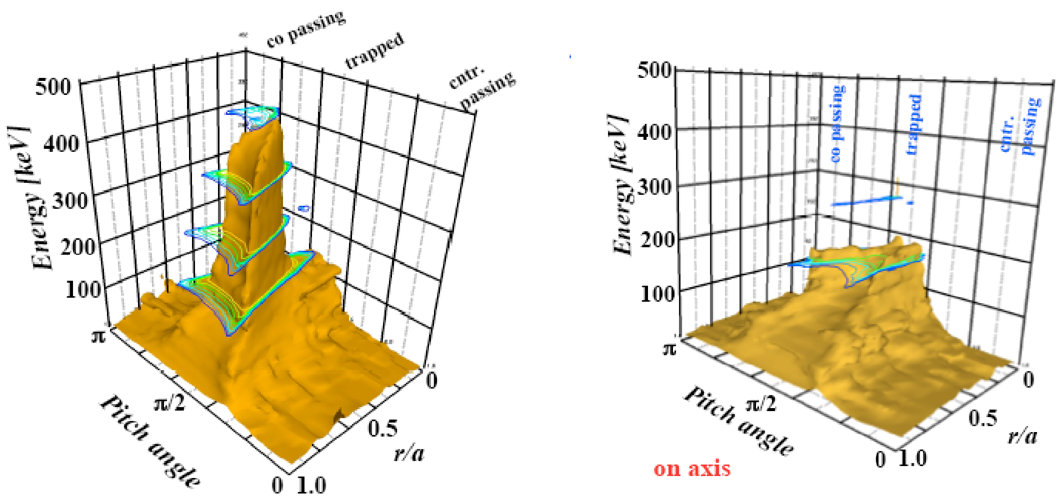

FIG. 3: Steady state distribution of energetic tail ions in the (r/a, E, pitch angle) space in the off-axis point heating case (left) and on-axis heating case (right).

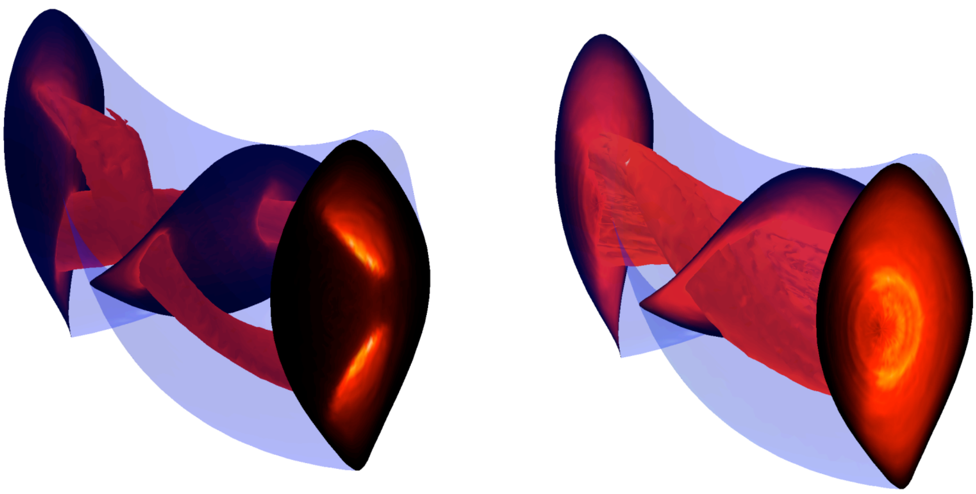

FIG. 4: 3D plots of the minority ion pressure in the off-axis point heating case (left) and on-axis heating case (right).

To understand this difference we plotted the resonance magnetic field strength with the modulation of magnetic field along the field line. Figure 5 shows the relative strength of the resonant magnetic field for two heating cases; the off-axis case (dotted line) and the on-axis heating case (dashed line).

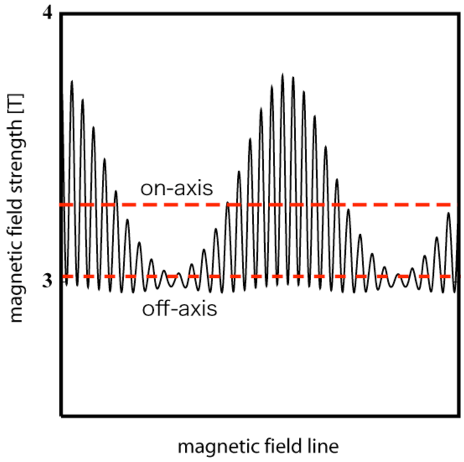

FIG. 5: Magnetic field strength along the field line at the flux surface of r/a=0.5.

The trapped particle whose banana tip is close to the resonance surface can absorb large energy from the RF wave. We can see, in the off-axis heating case, that the trapped particle absorbing large energy exists almost all region along the field line. This means that the those particle are resonate for a longer time and interact many times with the RF wave.

On the other hand the large absorbing trapped particle are a partly exist in the on-axis case. This means that the orbit of the large absorbing trapped particle is unstable and the transition between helically and toroidally trapped particles occurs. This transition takes place the stochastic behavior of the particle orbit and enhances the radial diffusion of energetic particles.

Therefore, we can conclude that the higher peak is observed in the distribution function in the off-axis case because the large absorbing trapped particles are more stable in the off-axis case than that of the on-axis heating case.

We can see the difference between two heating cases more clearly by the radial profile of the heating. Figure 6 shows the radial profiles of energetic ion pressure, heat deposition and minority ion density. The peaked pressure profile can be seen in the off axis case and the broader one is in the on-axis case. The heat deposition also shows the maximum near r/a=0.5 in the off-axis case and flat one in the on axis case. The estimated heating efficiencies are about 70% for both cases and the difference of the radial profile does not influence the heating efficiency.

It is also found that the minority ions are pumped out near r/a=0.5 in the off-axis case and near the axis in the on-axis case. These indicate that ICRF heating diffuse out the minority ions from the resonance layer.

To compare with the experimental results we have simulated the neutral count number detected by NDD-NPA using the simulation results. Relatively good agreement is obtained between the experimental and simulation results (Fig.7). Both the computed and the experimental counts have similar dependency on the energy spectrum.

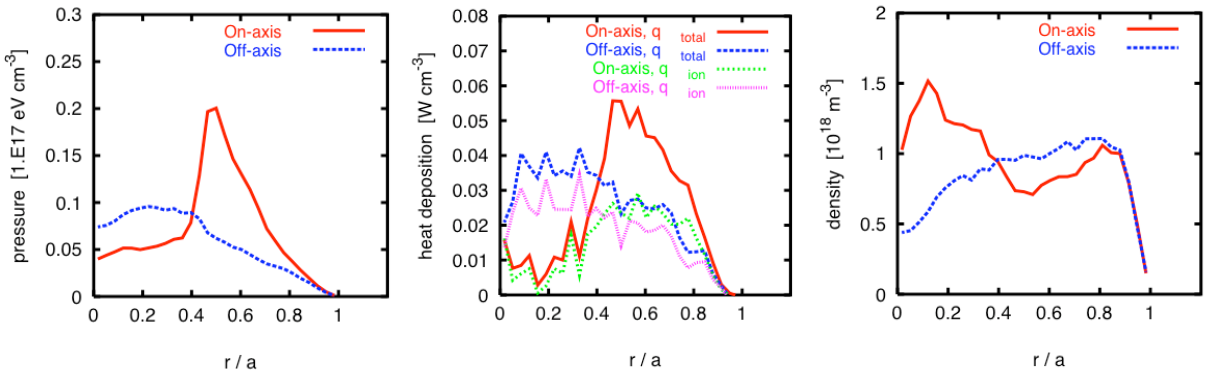

FIG. 6: Radial profiles of energetic ion pressure, heat deposition and minority ion density for the saddle point heating (red solid) and the on axis heating (blue dotted, closed).

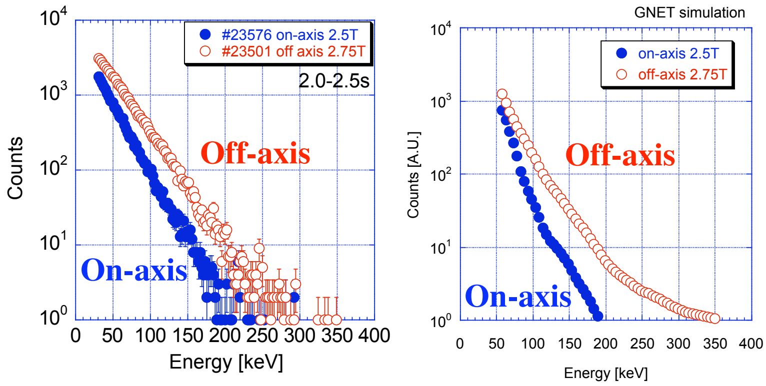

FIG. 7: Comparisons of the energy spectrum by the NDD-NPA results (left) and the simulation results (right) for the saddle point heating (red open) and the on axis heating (blue closed).

5. Conclusions

We have developed a global simulation code combining two code; GNET and TASK/WM. The GNET code solves a linearized drift kinetic equation for energetic ions including complicated behavior of trapped particles in 5-D phase space and the TASK/WM code solves Maxwell's equation for RF wave electric field with complex frequency as a boundary value problem in the 3D magnetic configuration.

The developed code has been applied to the analysis of energetic tail ion transport during ICRF heating in the LHD plasma. A steady state distribution of energetic tail ion has been obtained and the characteristics of distribution in the phase space are clarified. The resonance position dependency on the distribution have been shown and larger tail formation have been obtained in the off-axis heating case. This tendency agrees well with the experimental results. We have compared the GNET simulation results with the experimental results evaluating NDD count number and also obtained similar tendencies.

We have demonstrated that a global analysis is necessary for understanding the energetic particle transport in non-axisymmetric configurations.

References

[1] MUTOH, T., et al., Nucl. Fusion **24** (1984) 1003.
[2] NISHIMURA, K., et al., in Plasma Physics Controlled Nuclear Fusion Research 1994 (Proc. 15th Int. Conf. Seville, 1994), Vol. 1, IAEA, Vienna (1995) 679.
[3] OKADA, H., et al., Nucl. Fusion **36** (1996) 465.
[4] MASUDA, S., et al., Nucl. Fusion **37** (1997) 53.
[5] NOTERDAEME, J.-M., et al.,in Fusion Energy 1996 (Proc. 16th Int. Conf. Montreal, 1996) Vol. 3, IAEA, Vienna (1997) 335.
[6] HARTMANN, D.A., et al., Contr. Fusion Plasma Phys., Proc. 24th EPS Conf., Berchtesgaden (Germany, 1997) p1633.
[7] KWON, M., et al., Nucl. Fusion **32** (1992) 1225.
[8] MUTOH, T., et al, Phys. Rev. Lett. **85** (2000) 4530.
[9] KUMAZAEA, R., et al., Phys. Plasmas **8** (2001) 2139.
[10] WATARI, T., et al. Nucl. Fusion **41** (2001) 325.
[11] MUTOH, T., et al., Fusion Sci. Technol. **46** (2004) 175.
[12] KRASHILNIKOV, A.V., et al., Nucl. Fusion 42 (2002) 759.
[13] SAIDA, T., et al., Nuclear Fusion **44** (2004) 488.
[14] MURAKAMI, S., et al, Nuclear Fusion **34** (1994) 913.
[15] MURAKAMI, S., et al, Nuclear Fusion **40** (2000) 693.
[16] MURAKAMI, S., et al., Fusion Sci. Technol. **46** (2004) 241.
[17] FUKUYAMA, A., YOKOTA, E., AKUTSU, T., Proc. 18th IAEA Conf. on Fusion Energy (Sorrento, Italy, 2000) **THP2-26**.
[18] CHOI, M., et.al., AIP Proceeding of the 15th Topical Conference in Radio Frequency Power in Plasmas 694 (2003) 86.
[19] MURAKAMI, S., et al., Nucl. Fusion **42** (2002) L19.
[20] ISOBE, M., et al., Rev. Sci. Instrum. **72** (2001) 611.